REVIEW

Check for updates

All-alkynyl-protected coinage metal nanoclusters: from synthesis to electrocatalytic CO_2 reduction applications

Leyi Chen, Lei Wang, Quanli Shen, Yonggang Liu and Zhenghua Tang [iD] *

Atomically precise metal nanoclusters have been attracting considerable research interests in the last two decades, thanks to their quantum confinement effect and molecule-like properties. Such properties are significantly affected, if not dominated, by the interfacial metal–ligand bonding motifs. Recently, ligand engineering has been applied to alkynyl molecules, as they can bind to metal atoms with σ and/or π bonds, yielding versatile interfacial bonding motifs hence drastically different properties and functionalities can be realized, as compared to the most commonly employed thiolate ligands. This review first describes the unique advantages of alkynyl-protected metal nanoclusters, with elaboration on the comparison of the interfacial coordination mode and the optical features between thiolate/alkynyl protection. Following that, the recent progress regarding the synthetic strategy is discussed, with an emphasis on the direction reduction method and the synchronous nucleation and passivation strategy. Next, alkynyl-protected metal nanoclusters for the electrochemical CO_2 reduction reaction (eCO_2RR) are mainly discussed, with some explicit examples to elucidate the metal core effect and surface ligand effect as well as to explain the structure–performance relationship. At last, the challenges and perspectives from synthesis to the eCO_2RR of alkynyl-protected metal nanoclusters are proposed. We envision this review to stimulate more research efforts to be dedicated to developing effective synthetic strategies and advancing the catalytic mechanistic understanding of alkynyl-protected metal nanoclusters toward the eCO_2RR and beyond.

1. Introduction

1.1. Why study alkynyl-protected metal nanoclusters?

Coinage metal (Au, Ag, Cu, *etc.*) nanoclusters with an ultrasmall size (usually below 3.0 nm) hold a unique position in the field of nanomaterials, as they possess significantly different optical properties and electronic and microscopic structural features because of the relatively large nanoparticles or nanocrystals thanks to their strong quantum confinement effect.[1–3] Such an effect of the metal nanoclusters also leads to their application as antibacterial agents[12,13] and versatile applications in various fields, such as photo/electrocatalysis,[4,5] environmental remediation,[6,7] sensing,[8,9] bioimaging or biolabeling,[10,11] and so on. More importantly, metal nanoclusters can be chemically synthesized with molecular purity, that is, atomic precision. Atomically precise metal nanoclusters have a well-defined size, a crystallographically resolved structure, and a definitive coordination environment at the atomic level, hence they play a critical role in the fundamental

nanoscience study, because they can serve as a model to correlate the structure–property/performance relationship. In most cases, metal nanoclusters hold a spherical core@shell configuration,[14–16] where a few or tens of metal atoms are arranged in a certain pattern in the core and the ligand molecules are capped onto the metal core as the protective shell.[17–19]

The surface ligands coordinate with a certain portion of core metal atoms to form some interfacial bonding motifs, which affect if not dominate the physicochemical properties of metal nanoclusters. Currently, thiolate molecules,[20–22] phosphine,[17,23] halogen,[24,25] *N*-heterocyclic carbenes,[26,27] and other organic compounds[28,29] have been widely employed to stabilize the metal core to form a large quantity of molecular metal nanoclusters. Recently, alkynyl ligands have been continuously gaining increasing research attention thanks to their characteristic binding patterns with surface metal atoms.[30–33] For instance, compared with the most extensively employed thiolate molecules, alkynyl molecules can form σ and/or π bonding with Au or Ag atoms,[34,35] yielding more diverse interfacial bonding motifs, which endow alkynyl-protected coinage metal nanoclusters with drastic physicochemical properties and functionalities.

New Energy Research Institute, School of Environment and Energy, South China University of Technology, Guangzhou Higher Education Mega Centre, Guangzhou, 510006, China. E-mail: zhht@scut.edu.cn
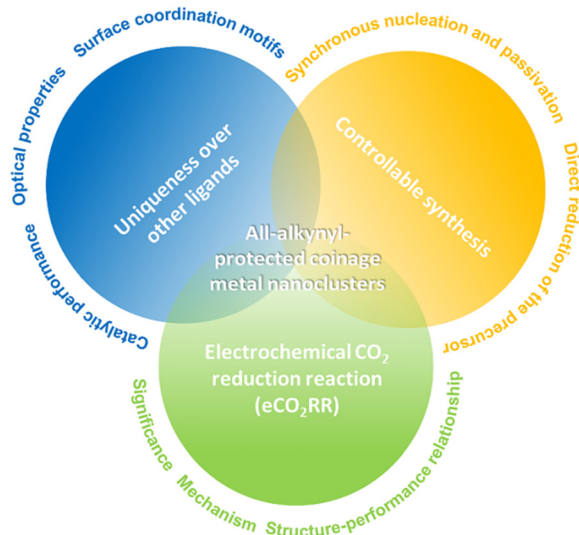
Fig. 1 The main content in this review regarding all-alkynyl-protected metal nanoclusters.
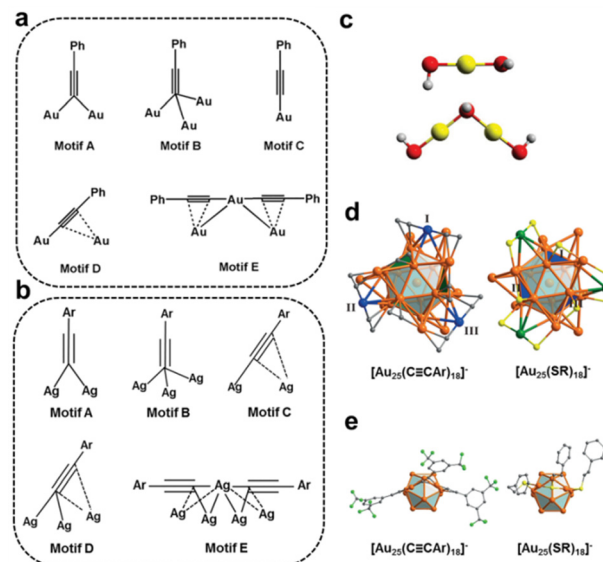

Fig. 2 Fundamental coordination modes of alkynyl ligands on (a) Au atoms and (b) Ag atoms. (c) Essential bonding modes of thiolate ligands on metal atoms. Comparison of the geometric configurations of (d) V-shaped staples and (e) surface motifs on $[Au_{25}(C\equiv CAr)_{18}]^-$ and $[Au_{25}(SR)_{18}]^-$. Copyright 2018, American Chemical Society and Wiley,[34,38] and Copyright 2020, Wiley.[36]

As illustrated in Fig. 1, this review first emphasizes the uniqueness of alkynyl ligands over other ligands for preparing metal nanoclusters, with a particular focus on surface coordination motifs, optical properties, and catalytic performance. Following that, the controllable synthesis of molecular alkynyl-protected metal nanoclusters is discussed, mainly elaborating on the direct reduction (DR) method and the synchronous nucleation and passivation (SNP) strategy. Final and the major part is regarding atomically precise alkynyl-protected metal nanoclusters for the electrochemical CO_2 reduction reaction (eCO$_2$RR), involving the significance and mechanism of eCO$_2$RR and some explicit examples for elucidating the structure–performance relationship.

1.2. The comparison of alkynyl ligand *vs.* thiolate ligand protected nanoclusters

1.2.1. The comparison of coordination modes. The coordination modes of an alkynyl molecule on a metal surface are more variable due to the $C\equiv C$ bond, as the terminal C atom can attach to the metal core by forming a σ bond, while the $C\equiv C$ bond can coordinate the metal atom in the form of π bonding. For example, the interfacial binding motifs of alkynyl-protected Au nanoclusters can be divided into the five essential types:[34] μ_1-η^1; μ_2-η^1, η^1; μ_3-η^1, η^1, η^1; μ_2-η^1, η^2 and linear PhC$\equiv$C–Au–C$\equiv$CPh (Fig. 2a), much more diverse and complex than the thiolate-protected Au nanoclusters, which has only roughly two types of binding motifs,[36] that is, linear RS–Au–SR, and lengthened RS–Au–SR–Au–SR (Fig. 2c). For Ag nanoclusters, there are more diverse approaches for alkynyl molecules to coordinate with Ag atoms.[32,37] As illustrated in Fig. 2b, in motifs C, D, and E, the –C$\equiv$C–R group can bind to Ag than Au at least one or even two more metal atoms. Such a much more diverse binding behaviour from alkynyl molecules than thiolate ligands might be favourable for catalysis.

The structure comparison of $[Au_{25}(C\equiv CAr)_{18}]^-$ and $[Au_{25}(SR)_{18}]^-$ is an explicit example.[38] Both clusters have Au$_{13}$ icosahedra capped by six Au$_2$L$_3$ units with similar arrangements. Even if the six V-shaped $[Au_2(C\equiv CAr)_3]$ staples in $[Au_{25}(C\equiv CAr)_{18}]^-$ are similar to $[Au_2(SR)_3]$ in $[Au_{25}(SR)_{18}]^-$, the connection to the Au$_{13}$ kernel is quite different. Three Au atoms in V-shaped staples (labelled in blue, Fig. 2d) of $[Au_{25}(C\equiv CAr)_{18}]^-$ are twisted about 60°, referring to that in $[Au_{25}(SR)_{18}]^-$ (labelled in green, Fig. 2d), resulting in the two Au atoms in $[Au_2(C\equiv CAr)_3]$ capping the adjacent triangular pattern, while two Au atoms in $[Au_2(SR)_3]$ are capped by the uniformly distributed triangles. Moreover, it also leads to $[Au_{25}(C\equiv CAr)_{18}]^-$ being present as a racemate. In addition, the angle between the terminal C$\equiv$C to Au atom is about 180°, while the angle of C–S–Au is less than 106° (Fig. 2e). This case exemplifies that the alkynyl ligand significantly affects the metal core configuration of the coinage metal nanoclusters.

1.2.2. The comparison of optical properties. As the ligand interacts with a significant amount of metal core atoms of the nanocluster, it plays a critical role in modulating the electronic structure of the metal nanoclusters. For instance, the optical absorbance feature of alkynyl-protected metal nanoclusters is (drastically) different from other ligand capped nanoclusters. As shown in Fig. 3a, both alkynyl-protected and thiolate protected Au$_{25}$ nanoclusters have a broad peak at ∼700 nm, and all the other peaks from the alkynyl-protected Au$_{25}$ molecules are red-shifted about 50 nm compared to thiolate protected Au$_{25}$ nanoclusters.[38] Fig. 3b compares the absorbance spectra between the alkynyl and thiolate protected Au$_{36}$ nanoclusters. Au$_{36}$(SR)$_{24}$ displays multiple absorbance peaks, and in stark contrast, a significant red shift in the wavelength region beyond
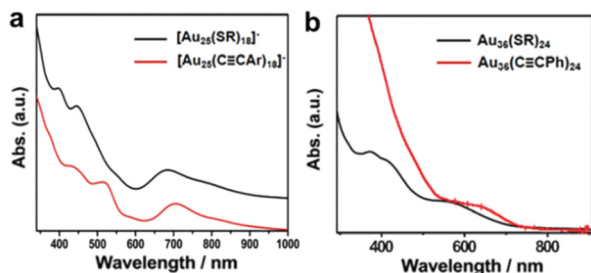
Fig. 3 The comparison of optical properties of (a) $[Au_{25}(PhC{\equiv}CAr)_{18}]^{-}$, $[Au_{25}(SR)_{18}]^{-}$and (b) $Au_{36}(PhC{\equiv}C)_{24}$, $Au_{36}(SR)_{24}$. Copyright 2017 and 2018, Wiley.[38,39]

500 nm is observed for $Au_{36}(PhC{\equiv}C)_{24}$ and the intensity of the characteristic peaks in the low wavelength is strongly reduced even disappears to some extent.[39]

In addition to the optical absorption feature, alkynyl molecules can also affect the luminescence properties of the metal nanoclusters, *e.g.* the photoluminescent behaviour and the corresponding quantum yield. For example, Konishi *et al.* reported that, despite the photoluminescence spectra of $[Au_{13}(dppe)_5(C{\equiv}CPh)_2](PF_6)_3$ is similar to that of $[Au_{13}(dppe)_5Cl_2](PF_6)_3$, the quantum yield of the former one (0.16) is significantly higher than that of the latter one (0.11).[40] The Wang group discovered that, $Au_{22}(^tBuC{\equiv}C)_{18}$ has a strong luminescence in the solid state with a quantum yield of 15%, and interestingly, it displays thermochromic luminescence.[41] By using the chiral alkynyl group, the Zang group fabricated a new enantiomeric pair of superatomic Ag_{17} nanoclusters, and both molecules emit near-infrared light with a quantum yield of 8.0% under ambient conditions as well as NIR circularly polarized luminescence thanks to the chirality of the excited states.[42] The emission colour of $Ag_{51}(^tBuC{\equiv}C)_{32}$ reported by Lu and Xie groups can change from blue to red by changing the solvent polarity from the less polar dichloromethane to the more polar methanol, exhibiting a strong solvatochromic effect.[43]

1.2.3. The comparison of catalytic performance. As the electronic structure and physiochemical properties of metal nanoclusters can be affected by the surface ligand, engineering the surface ligand can fine-tune the catalytic performance of the metal nanoclusters. Specifically, once the alkynyl molecules are attached onto the metal core to form a large $-C{\equiv}C-M$ (M = metal) conjugated system, it favours the electron shuttling and hence promotes the catalytic performance for certain reactions. For instance, Wan *et al.* reported that, in alkyne semi-hydrogenation catalysis, the conversion rate of $[Au_{38}(L)_{20}(Ph_3P)_4]^{2+}$ (L = alkynyl ligands) as catalyst reached up to 97%, while that of thiolate stabilized Au_{38} with the same core structure was less than 2%.[44] Such a ligand effect also occurs in the hydrogen evolution reaction (HER). The Tsukuda group found that, the onset potential of hydrogen evolution for $Au_{25}(C{\equiv}CAr^F)_{18}$ was about 70 mV positive than that of $Au_{25}(SC_2H_4Ph)_{18}$ under the same conditions, indicating that alkynyl ligands significantly enhanced the HER activity.[45]

2. Controllable synthesis

Since the seminal Brust method was reported for preparing monodisperse nanoclusters in 1994, various strategies have been developed for the controllable synthesis of metal nanoclusters with molecular purity. For alkynyl-protected metal nanoclusters, the applicable synthetic methods include a direct reduction (DR) of the precursor,[39,46] synchronous nucleation and passivation (SNP),[37,47,48] ligand exchange,[40,49,50] one-pot method[41,51,52] and so on (Fig. 4). With these methods on hand, plus the advancement of crystallographic techniques, a great deal of all-alkynyl-protected Au, Ag, and AuAg alloy nanoclusters with crystal structures have been recorded. This review will mainly discuss the DR method and SNP strategy.

2.1. Direct reduction of the precursor

Direct reduction (DR) of the precursor is the most facile and straightforward method to fabricate metal nanoclusters, but manipulating the reaction kinetics to obtain a monodisperse product is quite challenging. Currently, the DR approach is the most widely employed strategy to acquire alkynyl-protected metal nanoclusters. Specifically, metal salts (*e.g.* Me_2SAuCl,[30,53,54] Ag_2O[31,55]) were first reacted with the alkynyl ligand to generate the $Au(I)/Ag(I)$-alkynyl complexes (the precursor), then the reducing agent (*e.g.* $NaBH_4$[43,56]) was added to reduce the precursor to form metal nanoclusters. In some cases, a mixture of cluster molecules is acquired, hence the post-synthetic isolation and purification are necessary. So far, Au_{42},[30] Au_{99},[53] Ag_{47},[31] Ag_{112},[32] and $Au_{34}Ag_{28}$[57] have been chemically prepared using this method.

It is worth noting that the morphology and aggregation state of the precursor can be critical for forming the final product. Our group disclosed that, by introducing ethanol in the preparation of Au–PA (PA = phenylacetylene) precursor, the amorphous precursor can self-assemble into flower-like macromolecules[54]
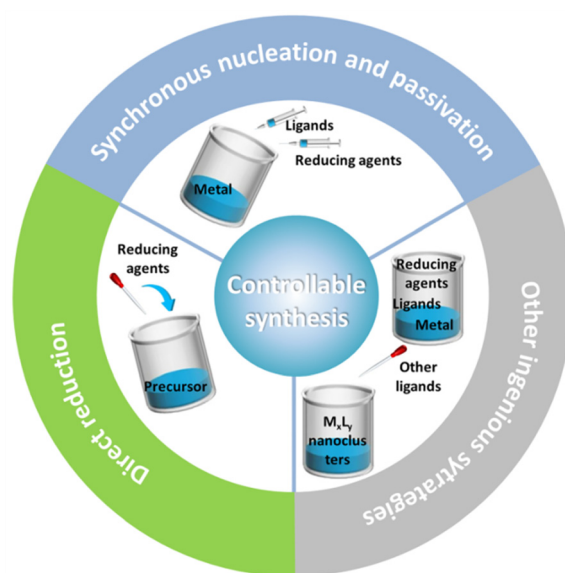

Fig. 4 Controllable synthesis strategies for all-alkynyl-protected metal nanoclusters.
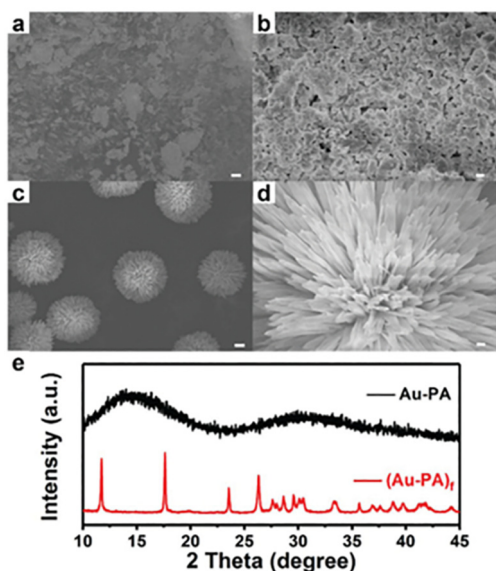
Fig. 5 SEM images of Au–PA precursors at (a) 5 μm, (b) 500 nm and (Au–PA)$_f$ precursors at (c) 5 μm, (d) 500 nm. (e) XRD patterns of the amorphous Au–PA precursor generated without ethanol and the flower-like (Au–PA)$_f$ precursor generated with the presence of ethanol. Copyright 2020, Royal Society of Chemistry.[54]

(Fig. 5, denoted as (Au–PA)$_f$). Consequently, compared with the amorphous precursor, the well-defined (Au–PA)$_f$ precursor can lead to the formation of Au$_{144}$(PA)$_{60}$ with higher yield and monodispersity. Such a phenomenon is reminiscent of the high-yield synthesis of Au$_{25}$(SR)$_{18}$, in which the monodisperse Au–SR precursor was obtained by controlling the reaction kinetics.[58]

2.2. Synchronous nucleation and passivation strategy

To form a nanocluster molecule, it undergoes nuclei growth and surface passivation process which compete with each other. For the DR approach, it might be difficult to manipulate these two processes to improve the yield of the target cluster. For instance, an excess amount of reducing agent may lead to excessive reducibility to form large nanoparticles spontaneously, while a rapid reduction rate may induce the surface passivation occurring inhomogeneously hence increasing the polydispersity of the product. From that, regulating the reaction rate and manipulating the reducing process might be critical for enhancing the yield of molecular metal nanoclusters.

In 2020, our group developed a synchronous nucleation and passivation strategy to fabricate Au$_{36}$(PA)$_{24}$ and Au$_{22}$(PA)$_{18}$ nanoclusters with a high yield of 17.1% and 70.1%, respectively.[47] In this method, the ligand and reducing agent were added simultaneously, and more importantly, NaBH$_3$CN instead of NaBH$_4$ was employed as the reductant, and the reaction was also conducted at a low temperature. By doing that, the cluster nuclei growth and surface ligand passivation can be more easily manipulated to obtain molecular metal nanoclusters. As illustrated in Fig. 6, the equivalent ratio of NaBH$_3$CN-to-Au is critical for yielding different products. When NaBH$_3$CN is much more excessive (eq ≫ 3), polydisperse Au
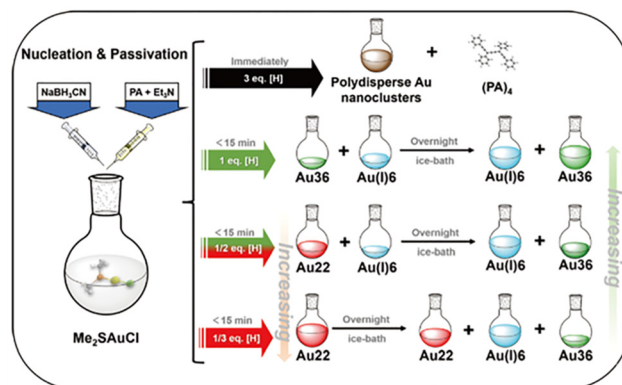

Fig. 6 Synthetic routes for Au$_{36}$(PA)$_{24}$ with the different amounts of reducing agents in the synchronous nucleation and passivation strategy. Copyright 2020, Springer.[47]

nanoclusters were acquired; when NaBH$_3$CN was decreased to a certain low amount (eq = 1/2, 1/3), Au$_{22}$(PA)$_{18}$ as the reaction intermediate formed, but it can transform into Au$_{36}$(PA)$_{24}$ overnight eventually. In this work, we also proposed the structure evolution from Au$_{22}$(PA)$_{18}$ to Au$_{36}$(PA)$_{24}$, and the calculated stoichiometric ratio of Au$_{22}$(PA)$_{18}$-to-Au$_{36}$(PA)$_{24}$ was verified by the designed experiment as well. Such synchronous nucleation and passivation strategy is of great universalities to prepare alkynyl-protected Ag, AuAg alloy nanoclusters, and in later studies, other molecules such as Ag$_{32}$,[37] and Au$_9$Ag$_9$[48] clusters were synthesized by this method with high yields.

2.3. Other ingenious synthesis strategies

Besides the above two approaches, there are some other ingenious strategies to synthesize homoleptic alkynyl-protected metal nanoclusters. One method is the ligand exchange reaction, in which another ligand is introduced into a solution of the parent cluster with high polydispersity or molecular purity to yield new cluster molecules.[59] Ligand exchange can transform the cluster size, morphology, composition, and structural arrangement and also introduce new chemical/physical properties.[49,60,61] Pioneering work using this method to prepare all-alkynyl-protected metal clusters was done by Tsukuda *et al.* In 2011, by reacting polyvinylpyrrolidone stabilized Au nanoclusters with a series of alkynyl molecules, several magic clusters such as Au$_{54}$(PA)$_{26}$, Au$_{94}$(PA)$_{38}$, and Au$_{110}$(PA)$_{40}$ can be identified in the mass spectra of the final mixture product.[62] In 2019, the same group reported a quasi ligand exchange reaction, in which hydride-doped [HM@Au$_8$-(PPh$_3$)$_8$]$^+$ (M = Pd, Pt) reacting with Au(ɪ)-alkynyl oligomer to yield [MAu$_{24}$(C ≡ CAr^F)$_{18}$]$^{2-}$ clusters.[63] Interestingly, Hosier *et al.* revealed that the simple thiolate-to-acetylide ligand exchange is enthalpically unfavorable, while metathesis reactions between these ligands are enthalpically favorable.[64] However, the direct reaction between phenylacetylene and thiolate Au clusters can not proceed, and the acetylide-for-thiolate ligand exchange is only facile when using either a gold(ɪ)–phenylacetylide complex or lithium phenylacetylide as an incoming ligand to thiolate protected Au clusters. From this point, using ligand exchange to prepare alkynyl-protected metal nanoclusters has been restricted to some extent.

Another strategy is the one-pot synthetic approach, which is quite straightforward and of easy operability. The most significant feature of this method is that all the reagents (the metal salt, the ligand, the reductant, *etc.*) were added together to react in one system, similar to SNP but with less kinetic control and easier to operate. For instance, the Tsukuda group fabricated a series of homoleptic alkynyl-protected $Au_{22}(C\equiv CR)_{18}$ cluster molecules protected with four different ligands by reacting $(Me_2S)AuCl$, the ligand, and triethylamine together.[51] Interestingly, triethylamine not only serves as a base, but also is the reducing agent, and its low reducing capability left $(Me_2S)AuCl$ not completely reduced, hence the yields of all the clusters were less than 8%. In another study, the Wang group synthesized a pair of $Au_{23}(C\equiv C^tBu)_{15}$ clusters (Au_{23}-1 and Au_{23}-2), which are the first isomers observed in all-alkynyl-protected metal nanoclusters.[52] Specifically, Au_{23}-1 was prepared by reduction of Me_2SAuCl and $HC\equiv C^tBu/Et_3N$ with $NaBH_4$, but Au_{23}-2 has to be acquired with a similar synthetic procedure in the presence of tetraphenylphosphonium chloride or tetrabutyl-ammonium chloride. The yield of Au_{23}-1 and Au_{23}-2 was 31% and 10%, respectively. It shows that, by optimizing the synthetic parameters, the one-pot method can obtain molecular metal nanoclusters with high yields, but more cases await to be explored.

3. Alkynyl-protected metal nanoclusters for eCO$_2$RR

3.1. The importance of eCO$_2$RR

Since the last century, the overuse of fossil fuels and rapid industrialization has caused serious greenhouse effects globally.[65] CO_2 is the major greenhouse gas, whose emission must be reduced to a certain minimum level to meet the framework of the Paris Agreement. Capturing, storing, and utilizing CO_2 is one of the effective means to mitigate the great CO_2 emission pressure.[66] Among that, electrochemical CO_2 reduction reaction (eCO$_2$RR) has been attracting increasing research attention recently, as it can convert CO_2 into valuable chemicals. More importantly, eCO$_2$RR can be conducted under mild conditions with high efficiency, and take advantage of renewable electricity.[67,68] However, the $C=O$ bond is difficult to be broken because it has large bond dissociation energy of 750 kJ mol^{-1}. Meanwhile, as it has multiple proton-coupled electron transfer steps with comparable potentials, plus the side reaction of hydrogen evolution, it is extremely challenging to control the product selectivity.[65] The presence of electrocatalysts can lower the energy barrier of eCO$_2$RR, but most of the electrocatalysts still suffer from high overpotential, low current density, and poor product selectivity.[69] Therefore, developing electrocatalysts with high efficiency, high activity and selectivity is imperative.

3.2. The mechanism of eCO$_2$RR

As multiple protons/electrons transfer are involved in eCO$_2$RR, the reaction pathway and mechanism of eCO$_2$RR are rather complicated. Based on the electron-transfer number, the reduction products can be classified into C_1 molecules such as CO, HCO_2H, CH_3OH, and C_{2+} molecules such as CH_3CH_2OH, CH_3CHO, C_2H_6, C_2H_4, *etc.* Regardless of the product generated, eCO$_2$RR follows the basic process: 1. Adsorption of CO_2 molecules on the catalyst surface; 2. Proton coupled electron transfer reactions of the intermediates; 3. Recombination of molecules and desorption from the surface.[70] As molecular Au/Ag nanoclusters mainly produce CO products, we here focus on 2e$^-$ reaction only. An important concept regarding the reaction process is the rate-determining step (RDS), which is defined as the step with the largest energy barrier in the process. The overall reaction rate is governed by the RDS.

The general mechanism of the 2e$^-$ reaction is presented in Fig. 7. Generally, the *COOH formation is the key step for producing CO, and there are two pathways to form *COOH. In one way, CO_2 grasps an electron to transform into *CO$_2^-$ and then obtains a proton to produce *COOH, while in another way, CO_2 directly combines with a pair of proton and electron (H^+/e^-) on the catalyst surface to form *COOH. CO and H_2O are the products once *COOH reacts with a pair of H^+/e^-. From *CO, CH_3OH and CH_4 can also be yielded, depending on the number of electron pairs. The formation of HCO_2H also has two possible pathways. On the one hand, the protonation of *CO$_2^-$ generates *OCHO first and *OCHO gets a pair of H^+/e^- to form HCO_2H. On the other hand, CO_2 interacts with H which is pre-adsorbed on the catalyst surface by a pair of H^+/e^- to form *HCOO, and then HCO_2H is produced through reacting with a pair of H^+/e^-.[65] In addition, density functional theory (DFT) calculations help to visualize the reaction path of eCO$_2$RR and the required energy to produce various intermediates, specific examples will be discussed in detail below.

3.3. Alkynyl-protected metal nanoclusters for eCO$_2$RR

Metal nanoclusters especially Au and Au-alloy nanoclusters have been widely employed as eCO$_2$RR catalysts, thanks to the unique advantages that are not available from nanoparticle counterparts. First of all, the molecule-like transition of metal nanoclusters can facilitate the electron transfer to the electrode and reactant hence decreasing the overpotential; secondly, metal nanocluster has tunable and versatile chemical functionalities, *e.g.* by tuning the size, surface ligand, charge state, doping another metal, and structure engineering, the redox potential can be manipulated to enhance the catalytic performance. Finally and most importantly, metal nanoclusters have
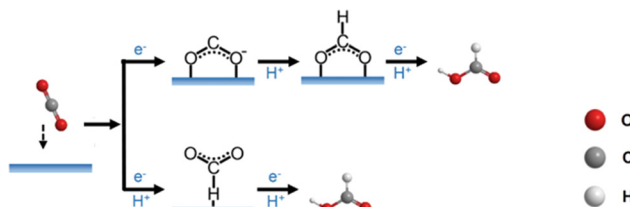

Fig. 7 Schematic diagram of the 2e$^-$ reaction path in eCO$_2$RR. Copyright 2021, Elsevier.[65]

a well-defined molecular structure with atomic precision, which is quite favourable for theoretically simulating the experimental findings to unravel the reaction mechanism and disclose the catalytic reaction center, hence establishing the structure–performance relationship eventually.[67]

So far, Au nanoclusters capped by all kinds of ligands (*e.g.* thiolate,[71,72] phosphine,[27] hydrides,[73] NHC,[74] and alkynyl[75,76]) especially thiolate molecules have been studied for eCO_2RR. Pioneering work has been conducted on thiolate-stabilized molecular Au nanoclusters by Jin groups,[77–80] and multiple groups have also made significant contributions.[81–84] Other ligands and mixed ligands protected Au nanoclusters also exhibited impressive performance toward eCO_2RR.[73] For instance, the Wang group reported that the mixed ligand capped $[Au_{55}(p\text{-}MBT)_{24}(Ph_3P)_6](SbF_6)_3$ (Au_{55}) can reach the highest FE_{CO} of 94.1% at −0.6 V with the maximal CO production rate of 50.34 μL min^{-1} at −0.9 V. Moreover, the Au_{55} catalyst exhibited good stability for over 4 h. The authors attributed the good catalytic properties to the ultrasmall size of the Au_{55} cluster, the corner Au atom, and the hydrophobic nature of the ligand.[85] In another study, the same group developed all-amidinate-protected $[Au_{28}(Ph\text{-}form)_{12}](OTf)_2$ clusters loaded on carbon nanotubes as a catalyst, which showed the maximal FE_{CO} of 97.5% at −0.57 V, and can still maintain over 91% for 40 h at −0.69 V in eCO_2RR.[86]

Recent high-quality review papers regarding metal nanoclusters for eCO_2RR mainly focus on the thiolate ligand, whereas a systematic summary of alkynyl-protected metal clusters for eCO_2RR is missing.[67,87,88] Here, we mainly discuss all-alkynyl-protected Au and Ag nanoclusters for eCO_2RR, with particular attention on elucidating the metal core effect and the surface ligand effect.

3.3.1. Metal core effects. Given the uniqueness of alkynyl ligands over thiolate molecules mentioned in Section 1.2, we tend to believe alkynyl-protected metal nanoclusters might be more favourable for eCO_2RR. Nevertheless, rare reports can be found on alkynyl-protected Au or Ag nanoclusters for the eCO_2RR.

In 2021, our group reported the structure analysis and eCO_2RR performance of the smallest all-alkynyl-protected $[Ag_{15}(C\equiv C^tBu)_{12}]^+$ (abbreviated as Ag_{15}) nanocluster.[89] As shown in Fig. 8a, Ag_{15} possesses a body-centered-cubic (bcc) structure with an $Ag@Ag_8@Ag_6$ metal core configuration. Interestingly, the two diagonal Ag atoms in the Ag_8 cube can connect to the two O atoms of the CO_2 molecule at two opposite sides, making the Ag_8 cube elongated and the Ag_{15} nanocluster assembled into one-dimensional material (Fig. 8b). Interestingly, Ag_{15} exhibited excellent catalytic activity toward eCO_2RR with CO as the main product and H_2 evolution is significantly suppressed, and the maximum FE_{CO} can reach *ca.* 95% at -0.6 V (Fig. 8c). In addition, the Ag_{15} catalyst can maintain good stability over 10 h (Fig. 8d).

DFT calculations were further conducted to determine the catalytic site and compare the catalytic selectivity of eCO_2RR to CO *vs.* H_2 evolution. The methyl group was used to replace the *tert*-butyl group to simplify the calculations, and one ligand
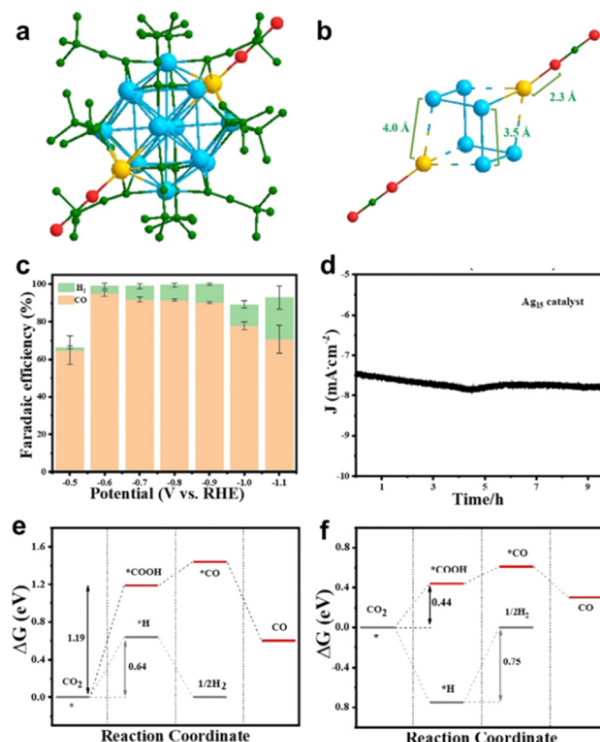

Fig. 8 Diagram of CO_2 adsorption on (a) $[Ag_{15}(C\equiv C^tBu)_{12}]^+$ and (b) Ag_8 cube. (c) Faradaic efficiency of CO and (d) stability testing of $[Ag_{15}(C\equiv C^tBu)_{12}]^+$. Comparison of free energy of electroreduction of CO_2 to CO process on (e) $[Ag_{15}(C\equiv C\text{–}CH_3)_{12}]^+$ and (f) $[Ag_{15}(C\equiv C\text{–}CH_3)_{11}]^+$. Copyright 2021, Wiley.[89]

stripping to expose the undercoordinated metal atom serves as the active site. For both the intact $[Ag_{15}(C\equiv C\text{–}CH_3)_{12}]^+$ cluster and one ligand stripped $[Ag_{15}(C\equiv C\text{–}CH_3)_{11}]^+$, the formation of *COOH is the rate determining step (RDS). As shown in Fig. 8e and f, $[Ag_{15}(C\equiv C\text{–}CH_3)_{11}]^+$ has much lower free energy (0.44 eV) to form *COOH rather than $[Ag_{15}(C\equiv C\text{–}CH_3)_{12}]^+$ (1.19 eV). Correspondingly, $[Ag_{15}(C\equiv C\text{–}CH_3)_{11}]^+$ has higher energy barrier for H_2 evolution than $[Ag_{15}(C\equiv C\text{–}CH_3)_{12}]^+$. Moreover, the energy barrier for *H formation is much larger than forming *COOH for $[Ag_{15}(C\equiv C\text{–}CH_3)_{11}]^+$, suggesting H_2 generation can be largely restricted. On the intact $[Ag_{15}(C\equiv C\text{–}CH_3)_{12}]^+$ cluster, the staple Ag atom acts as the active site for eCO_2RR, while in the one-ligand removed $[Ag_{15}(C\equiv C\text{–}CH_3)_{11}]^+$, the loss of one ligand causes 4 shell-Ag atoms to expose two equivalent triangular faces, in which one under-coordinated Ag atom prefers to CO_2 adsorption and reduction. This study manifests that the alkynyl-protected Ag nanocluster holds great potential for the eCO_2RR in terms of activity and stability and can advance the fundamental understanding of the eCO_2RR catalyzed by alkynyl-protected metal nanoclusters.

Doping another metal into the metal core to form bimetallic nanoclusters can alter the physiochemical properties of the clusters and lead to enhanced catalytic performance due to the synergistic catalytic effect.[90–92] The well-defined $Ag@Ag_8@Ag_6$ metal core structure of the Ag_{15} nanocluster allows us to conduct such metal exchange to tune and optimize the eCO_2RR

performance. In a following study, through the metal exchange, our group first prepared the $[Au_7Ag_8(^tBuC\equiv C)_{12}]^+$ (Au_7Ag_8 in short) cluster, of which the optical feature and crystal structure agree well with the previous report from Zheng group.[93] Meanwhile, the $[Ag_9Cu_6(^tBuC\equiv C)_{12}]^+$ (Ag_9Cu_6 in short) cluster was also synthesized *via* a one-pot strategy, and it displayed significantly different optical properties and chemical stability from Au_7Ag_8.[94] Furthermore, the $[Au_2Ag_8Cu_5(^tBuC\equiv C)_{12}]^+$ cluster ($Au_2Ag_8Cu_5$ in short) was also prepared by a metal exchange approach from Ag_9Cu_6.[95]

It is worth noting that, Au_7Ag_8, Ag_9Cu_6, and $Au_2Ag_8Cu_5$ are all M_{15} clusters with a similar metal core configuration. As demonstrated in Fig. 9a, they all possess an $M@M_8@M_6$ metal core, with one metal atom in the center, an M_8 cube in the middle layer, and an M_6 octahedron in the outmost layer in the core. Interestingly, the three clusters exhibited drastically different catalytic performances toward eCO_2RR. Au_7Ag_8 presented high selectivity for CO formation (Fig. 9b), with the highest FE_{CO} of 98.1% at −0.49 V. For both Ag_9Cu_6 and $Au_2Ag_8Cu_5$, CO and formate are the main products, despite the FE_{CO} showed a similar volcanic shape with Au_7Ag_8 and the highest FE_{CO} can reach 94.1% and 95.0% at −0.49 V for Ag_9Cu_6 and $Au_2Ag_8Cu_5$, respectively, the FE_{CO} decreased rapidly when the potential goes more negatively (Fig. 9b). Fig. 9c depicts $FE_{formate}$ of Ag_9Cu_6, and $Au_2Ag_8Cu_5$. When the potential goes negative, $FE_{formate}$ of Ag_9Cu_6 kept increasing while $FE_{formate}$ of $Au_2Ag_8Cu_5$ first increased gradually and then decreased. The maximal $FE_{formate}$ value for Ag_9Cu_6 and $Au_2Ag_8Cu_5$ is 47.0% at −1.19 V and 28.3% at −0.99 V, respectively. In addition, the highest $FE_{CO+formate}$ for Ag_9Cu_6 and $Au_2Ag_8Cu_5$ is ∼100.0% and ∼97.4%, suggesting both clusters were able to convert CO_2 into valuable chemicals. Meanwhile, both Au_7Ag_8 and Ag_9Cu_6 can suppress H_2 evolution, while at a higher negative potential range, HER gradually becomes dominant for $Au_2Ag_8Cu_5$ (Fig. 9d). Correspondingly, both Au_7Ag_8 and Ag_9Cu_6 exhibited robust stability while $Au_2Ag_8Cu_5$ showed slightly inferior long-term durability than the above two clusters, probably due to its metal core ($Au_1@Au_1Ag_4Cu_3@Ag_4Cu_2$) is slightly asymmetric.

By using the simplified single-crystal structures to build models, DFT calculations were next conducted to unravel the

reaction mechanism. The eCO_2RR and HER compete at the same metal site, specifically, Au for Au_7Ag_8, Cu for Ag_9Cu_6, and for $Au_2Ag_8Cu_5$, the staple Cu acts as the active site for HCOO* binding, while *COOH, *CO, and *H tend to bind with the sub-surface Au atom. It is predicted that one ligand stripping to expose the metal atom is the active center. For the intact Au_7Ag_8 cluster, the energy barrier to form *H (0.88 eV) is lower than that of forming *COOH (1.08 eV, Fig. 10a) hence not favours eCO_2RR. However, once one ligand is stripped, trans-COOH* prefers to bind to the undercoordinated Ag atom and ΔG significantly decreases to 0.47 eV, much lower than ΔG for desorption of *H (1.07 eV) hence eCO_2RR is quite favourable (Fig. 10b). For the Ag_9Cu_6 cluster, eCO_2RR and HER compete at the Cu site regardless of the structural integrity. As shown in Fig. 10c, the RDS for CO generation is forming *COOH (ΔG = 0.43 eV), and the RDS for formate generation is *HCOO-to-HCOOH (ΔG = 0.46 eV), while after stripping a ligand, the value is changed into 0.40 eV and 0.54 eV (Fig. 10d), respectively. However, for the intact Ag_9Cu_6 cluster, the energy barrier for H_2 formation is only 0.14 eV, hence HER prevails. The reaction mechanism of $Au_2Ag_8Cu_5$ is rather complicated, and it turns out that the removal of one alkynyl ligand bonded to two Ag atoms near the shell Au atom is more thermodynamically supported. When the $Au_2Ag_8Cu_5$ cluster is intact, ΔG of the RDS in *COOH generation is 0.62 eV (Fig. 10e), rather larger than the corresponding RDS energy barrier when removing one ligand (Fig. 10f), suggesting that the latter one favours CO formation. Furthermore, for forming formate, the active site shifted from the Cu site to the Au site, and the RDS changed from *HCOO-to-HCOOH (0.67 eV) to the generation of *HCOO (0.44 eV). Such shift of the active site may be responsible for the decrease of formate selectivity of $Au_2Ag_8Cu_5$ compared to Ag_9Cu_6.

The series of the M_{15} clusters (Ag_{15}, Au_7Ag_8, Ag_9Cu_6, $Au_2Ag_8Cu_5$) with the identical ligand shell offers a good example to examine the metal core effect of alkynyl-protected metal nanoclusters. For both Ag_{15} and Au_7Ag_8, CO is formed exclusively with high selectivity. However, with the presence of Cu, formate can be produced by Ag_9Cu_6 and $Au_2Ag_8Cu_5$, and the two-atom-difference led to drastically different eCO_2RR
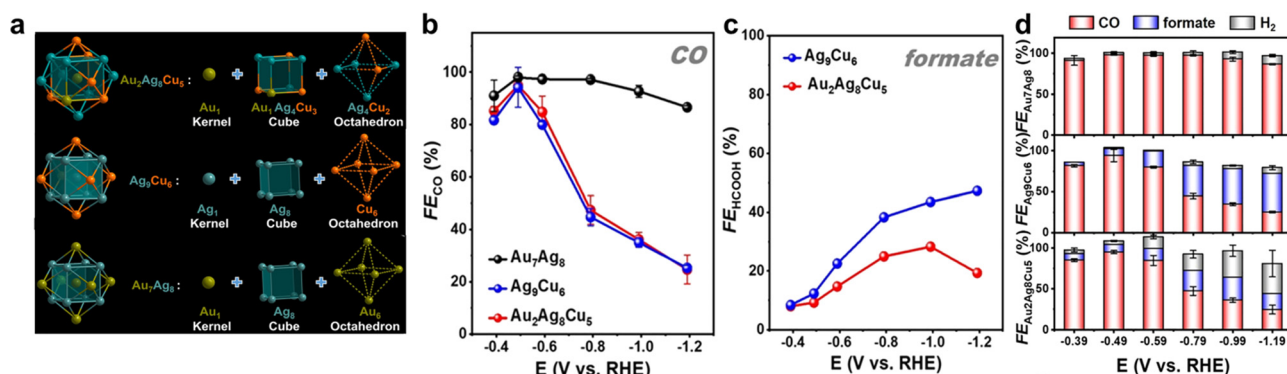

Fig. 9 (a) Structural anatomy of three nanoclusters. (b) FE_{CO} of three nanoclusters and (c) $FE_{formate}$ of $[Ag_9Cu_6(C\equiv C^tBu)_{12}]^+$, $[Au_2Ag_8Cu_5(C\equiv C^tBu)_{12}]^+$. (d) Product selectivity of three nanoclusters. Copyright 2022, Royal Society of Chemistry.[95]

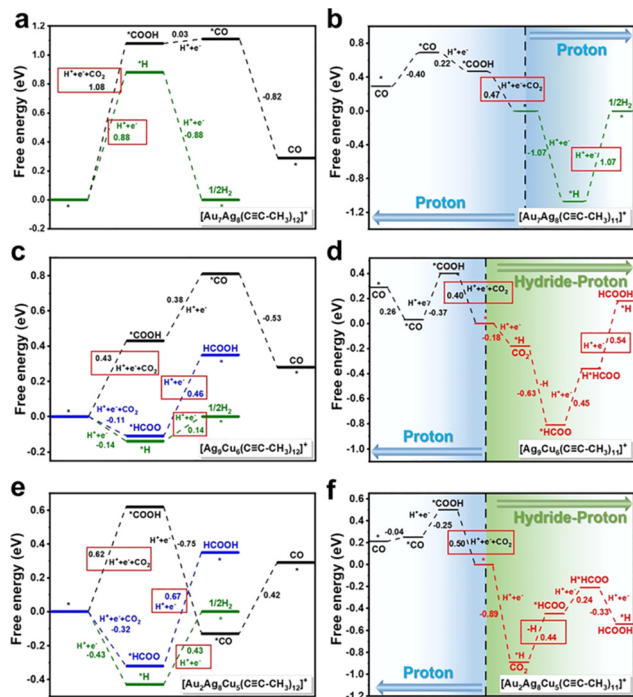**Fig. 10** Free energy of eCO_2RR and HER on (a) and (b) intact and incomplete Au_7Ag_8, (c) and (d) Ag_9Cu_6 and (e) and (f) $Au_2Ag_8Cu_5$. Copyright 2022, Royal Society of Chemistry.[95]

Fig. 11 The total structures of (a) $Au_{28}(C_2B_{10}H_{11}S)_{12}(tht)_4Cl_4$ and (b) $[Au_{28}(C_4B_{10}H_{11})_{12}(tht)_8]^{3+}$. (c) Faradaic efficiency of CO and (d) stability testing of two nanoclusters. Free energy of (e) eCO_2RR and (f) HER on $Au_{28}(C_2B_{10}H_{11}S)_{12}(tht)_4Cl_4$ (red) and $[Au_{28}(C_4B_{10}H_{11})_{12}(tht)_8]^{3+}$ (blue). Copyright 2022, Wiley.[97]

behaviours. Ag_9Cu_6 has higher $FE_{formate}$ than $Au_2Ag_8Cu_5$ at the applied potential, and at high negative potentials, the HER becomes dominant for $Au_2Ag_8Cu_5$. For Ag_{15} and Au_7Ag_8, one ligand stripping exposed the Ag and Au atom as the active site to form CO, respectively, while for Ag_9Cu_6 and $Au_2Ag_8Cu_5$, one ligand stripping exposed the Cu atom as the active site in the eCO_2RR, but the active site was shifted to the Au atom for producing formate for $Au_2Ag_8Cu_5$. That is, the exposed (111)-like Ag_2Cu_2 surface and the $Au_1Cu_1Ag_2$ surface are responsible for the markedly different eCO_2RR properties especially the selectivity of formate.

3.3.2. Ligand effects. The surface of the metal nanoclusters is capped by organic molecules, and these ligands can affect the physicochemical properties and electronic structure of the metal nanoclusters hence play a critical role in fine-tuning the electrocatalytic performance of the metal nanoclusters. For instance, an early study by the Jin group discovered that, compared to the phenylselenol (–SePh) protected Au_{25} cluster, the thiolate Au_{25} (–PET) cluster exhibited higher FE_{CO} and mass activity of CO while the former one exhibited higher FE_{H2}.[96] DFT calculations revealed that the breakage of ligand carbon tail to expose S/Se atoms as the active site. Due to the higher electron density, the S site is more favourable for forming the key intermediate of *COOH.

Recently, Wang *et al.* reported a ligand–shell engineering of Au_{28} clusters toward eCO_2RR, in which $Au_{28}(C_2B_{10}H_{11}S)_{12}$-$(tht)_4Cl_4$ (Au_{28}–S) and $[Au_{28}(C_4B_{10}H_{11})_{12}(tht)_8]^{3+}$ (Au_{28}–C) with the identical Au_{28} metal core showed different eCO_2RR performance.[97] Specifically, Au_{28}–S is co-protected by carbora-nethiolate, tetrahydrothiophene (tht), and chloride, while
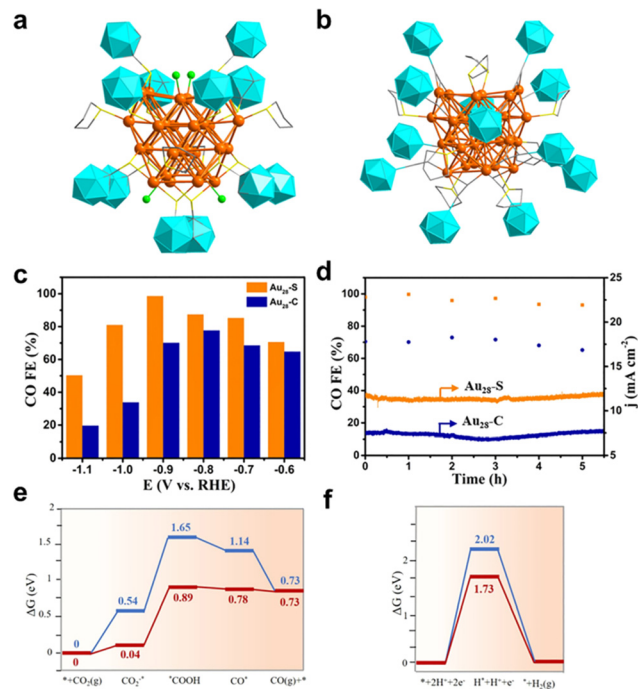
Au_{28}–C is co-protected by carboranealkynyl and tht ligands (Fig. 11a and b). Interestingly, despite the same metal kernel, the different protecting layer leads to the change in the overall electronic structure, *e.g.* Au_{28}–C has 13 valence electrons while Au_{28}–S has 12. In addition, compared to Au_{28}–C, the emission peak is blue-shifted at about 167 nm with the intensity increased about 5 times for Au_{28}–S. Furthermore, Au_{28}–S exhibited markedly superior eCO_2RR properties than Au_{28}–C. As illustrated in Fig. 11c, Au_{28}–S showed higher FE_{CO} values in all tested potentials, and it achieves the maximum FE_{CO} of 98.5% at −0.9 V, about 1.4 times than that of Au_{28}–C. However, both clusters exhibited satisfactory stability with a negligible change of FE_{CO} (Fig. 11d). *In situ* FTIR analysis shows that the intensity of the peaks at 1362 and 1636 cm^{-1} attributed to the *COOH species from Au_{28}–S is stronger than that from Au_{28}–C. Moreover, the authors conducted DFT calculations to unravel the active site and elucidate the reaction mechanism. For Au_{28}–C, the Au atoms in the linear $C_2B_{10}H_{11}$–C≡C–Au–C≡C–$C_2B_{10}H_{11}$ motifs are accessible for CO_2 molecules, while removing Cl atoms to expose Au atoms are probably the active center for Au_{28}–S. Both clusters adopt the $CO_2(g)$–*CO_2–*COOH–*CO–CO pathway, while the formation of *COOH is the rate-determining step. Au_{28}–C has a ΔG of 0.85 eV, much smaller than that of Au_{28}–C with 1.11 eV, while high ΔG of H* adsorption indicated that HER is unfavorable on both Au_{28}–S and Au_{28}–C (Fig. 11e and f), yet Au_{28}–S is even more unlikely for HER to occur.

In another recent study reported by our group, the surface ligand effect of Ag_{32} nanoclusters toward eCO_2RR has been

probed.[37] In this study, two metal clusters, a homoleptic alkynyl-protected $Ag_{32}L_{24}$ (L = 3,5-bis(trifluoromethylbenzene) acetylide, Ag_{32} in short) plus thiolate and phosphine co-protected $[Ag_{32}(DPPE)_5(SR)_{24}]^{2-}$ were prepared. Interestingly, thanks to the σ and/or π binding between Ag and the C≡C bond, Ag_{32} presented more versatile ligand–metal binding motifs than that of $[Ag_{32}(DPPE)_5(SR)_{24}]^{2-}$. Such structure difference leads to drastically different eCO_2RR performance. As demonstrated in Fig. 12a and b, in all the tested potentials, FE_{CO} of Ag_{32} is higher than that of $[Ag_{32}(DPPE)_5(SR)_{24}]^{2-}$. The highest FE_{CO} is 96.44% at −0.8 V for Ag_{32}, while in stark contrast, only a maximum of 56.67% can be achieved at −1.0 V for $[Ag_{32}(DPPE)_5(SR)_{24}]^{2-}$. Impressively, both samples exhibited excellent rather comparable stability for prolonged operation, as no significant current decrease was observed for 15 h (Fig. 12c). DFT calculations disclosed that, one ligand stripping to form $Ag_{32}L_{23}$ as the active center for Ag_{32}, however, for $[Ag_{32}(DPPE)_5(SR)_{24}]^-$, as the Ag–P bond strength is stronger than that of the Ag–S bond, one –SR ligand stripping to form $[Ag_{32}(DPPE)_5(SR)_{23}]^-$ as the active center. As depicted in Fig. 12d, the free energy profile shows that $[Ag_{32}(C≡C–CH_3)_{23}]^+$ has a smaller energy for forming *COOH (0.4 eV) rather than $[Ag_{32}(P_2C_2H_6)_5(SCH_3)_{23}]^-$ (0.5 eV); meanwhile, $[Ag_{32}(C≡C–CH_3)_{23}]^+$ has a larger thermodynamic barrier for H_2 formation from adsorbed H* (0.51 eV) compared to $[Ag_{32}(P_2C_2H_6)_5(SCH_3)_{23}]^-$ (0.05 eV), indicating a higher CO selectivity. This study indicates that, without the presence of an easy stripping ligand (e.g. halogen), with a similar metal kernel, the alkynyl-protected metal nanocluster might have better eCO_2RR performance than thiolate counterparts.

3.3.3. Other factors. There are other factors such as the metal–ligand motif arrangement can also affect the eCO_2RR performance. Recently, Zhu and Pei groups reported the evolution from superatomic $Au_{24}Ag_{20}$ monomers into molecular-like $Au_{43}Ag_{38}$ dimeric nanoclusters, whereas the monomeric and dimeric nanoclusters exhibited markedly different eCO_2RR performance.[75] Specifically, $Au_{24}Ag_{20}(C_{12}H_{13})_{24}Cl_2$ (abbreviated as $Au_{24}Ag_{20}$-1) was first obtained and it can transform into $Au_{43}Ag_{38}(C_{12}H_{13})_{36}Cl_{12}$ (abbreviated as $Au_{43}Ag_{38}$-1), while $Au_{24}Ag_{20}(C_9H_7)_{24}Cl_2$ (denoted as $Au_{24}Ag_{20}$-2) was acquired and it was further converted into $Au_{43}Ag_{38}(C_9H_7)_{36}Cl_9$ (denoted as $Au_{43}Ag_{38}$-2). The two $Au_{24}Ag_{20}$ monomer has the identical $Au_{12}@Ag_{20}$ metal kernel, which undergoes a self-assembly pathway to form a $Au_{12}@Ag_{19}$–Ag–$Au_{12}@Ag_{19}$ kernel, and forms two dimeric $Au_{43}Ag_{38}$ nanoclusters eventually (Fig. 13a). As shown in Fig. 13b, the monomers had higher current density than the dimers, while the CO partial current density followed the descending order of $Au_{24}Ag_{20}$-1 > $Au_{24}Ag_{20}$-2 > $Au_{43}Ag_{38}$-1 > $Au_{43}Ag_{38}$-2 (Fig. 13c). Notably, the monomers exhibited much higher FE_{CO} than the dimers in the potential range from −0.4 to −0.8 V (Fig. 13d and e). The authors ascribed the different catalytic performances to the atomic-packing structures (individual-core vs. dual-core) and surface motif arrangements (parallel vs. crossed).

Fig. 12 Faradaic efficiency of CO for (a) $Ag_{32}(C≡CAr^F)_{24}$ and (b) $[Ag_{32}(DPPE)_5(SR)_{24}]^{2-}$ at different potentials. (c) Stability testing of two nanoclusters. (d) Comparison of ΔG of eCO_2RR on $Ag_{32}(C≡CCH_3)_{24}$, $Ag_{32}(C≡CCH_3)_{23}$, $[Ag_{32}(P_2C_2H_6)_5(SCH_3)_{24}]^{2-}$ and $[Ag_{32}(P_2C_2H_6)_5(SCH_3)_{23}]^{2-}$ with the HER. Copyright 2022, Springer.[37]

Fig. 13 (a) Structural anatomy of four nanoclusters. (b) LSV curves and (c) the corresponding CO partial current density of the $Au_{24}Ag_{20}$ and $Au_{43}Ag_{38}$ nanoclusters. Faradaic efficiency for CO_2RR products obtained on (d) $Au_{24}Ag_{20}$ and (e) $Au_{43}Ag_{38}$ nanoclusters. Copyright 2022, Royal Society of Chemistry.[75]

4. Challenges and perspectives

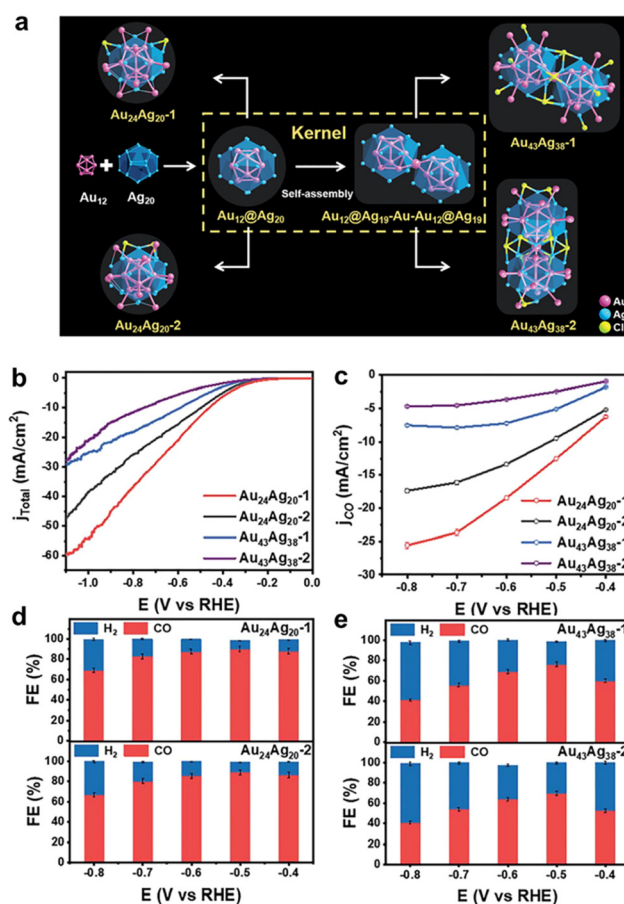In this review, we highlight the uniqueness of employing alkynyl molecules to prepare Au and Ag nanoclusters with atomic precision. Compared to thiolate molecules, the versatile binding motifs between alkynyl molecules and Au/Ag atoms facilitate the alkynyl-protected nanoclusters to possess drastically different optical properties, geometric configurations, and electronic structures. More intriguingly, significantly different catalytic performances can be achieved. The metal core effect and the surface ligand effect of the all-alkynyl-protected Au and Ag nanoclusters toward the eCO_2RR are discussed, demonstrating their great potential to modulate the performance through metal exchange or ligand shell engineering. Some conclusions and future perspectives can be drawn from the above discussions:

(1) Developing efficient synthetic methods with high yield to obtain more atomically precise alkynyl-protected metal nanoclusters is still highly desirable. Currently, in the case of Au and Ag, only Au_{22},[51] Au_{23},[52] Au_{36},[47] Au_{50},[30] Au_{67},[98] Au_{99},[53] Au_{110}[56] and Ag_{15},[89] Ag_{32},[37] Ag_{51},[43] and Ag_{74}[99] clusters with crystal structures have been documented. The case for Cu,[100] AuCu,[101] AgCu,[94] AuPd,[63] AuPt[45] and AgPt[102] is quite rare, and some (*e.g.* AgPd) are even missing. The family members of homoleptic alkynyl-protected metal nanoclusters need to be enriched. The direct reduction method is quite straightforward, but to control the monodispersity of the precursor is critical and deserves more research efforts. A synchronous nucleation and passivation strategy has proved its applicability for preparing single metal and some bimetallic nanoclusters with molecular purity, but more cases and examples need to be explored to confirm its generality. For ligand exchange and the one-pot method, more precise reaction condition control (*e.g.* the choice of introducing a ligand, the temperature, the concentration of the reactant, and the post-reaction purification) is essential to achieve precise synthesis;

(2) To obtain more valuable products from the eCO_2RR, synthesizing a Cu nanocluster or a Cu-alloy nanocluster is indispensable hence holds great potential. With Au and Ag nanoclusters as catalysts, CO is formed with high selectivity, and in the presence of Cu, HCO_2H can be acquired. So far, no C_{2+} products have been documented by coinage metal nanoclusters with atomic precision, regardless of the ligand type. In the presence of a hydride ligand for Cu nanoclusters, the negatively charged hydride plays a critical role in determining the selectivity, where HCO_2H is formed *via* the lattice-hydride mechanism.[103] The above case of all-alkynyl-protected Cu alloy clusters (Ag_9Cu_6, $Au_2Ag_8Cu_5$) shows that the HCO_2H formation occurs through a rather different proton-hydride mechanism or hydride-proton mechanism. Obtaining all-alkynyl-protected Cu nanoclusters for the eCO_2RR application would be of particular interest to advance the fundamental understanding of the eCO_2RR mechanism but still remains challenging, and Cu based bimetallic or trimetallic nanoclusters are also hoped to promote the activity and selectivity as well as to improve the mechanistic understanding.

(3) Advanced *in situ* techniques are urgently needed to examine the eCO_2RR process for gaining more mechanistic insights. For instance, DFT calculations predict one ligand stripping to expose undercoordinated metal atoms as the active site but losing several ligands might not necessarily favour the eCO_2RR reaction for the Ag_{15} cluster, and *in situ* techniques such as surface enhanced Raman scattering, infrared spectroscopy, high energy X-ray diffraction (XRD), extended X-ray absorption fine structure (EXAFS),[104] X-ray absorption near-edge structure (XANES),[104] small-angle neutron scattering (SANS)[105] *etc.* can provide some key structural information to confirm that. In addition, the *in situ* monitoring of the structural evolution of the catalyst during the eCO_2RR process may detect the metal–carbon cleavage, the adsorption configuration of CO_2 molecules on metal nanoclusters, the interaction between the cluster and the electrolyte, the real active site, the evolution of the key intermediates, and the formation process of the product more accurately.

In summary, with the advancement of synthetic methods, more molecular homoleptic alkynyl-protected metal nanoclusters with precise structures are anticipated to be discovered. The unique surface binding motifs and different physicochemical properties of the all-alkynyl-protected coinage metal nanoclusters can bring profound and valuable mechanistic insights of the eCO_2RR. We envision that increasing research efforts should be dedicated to this fundamentally interesting yet important field.

Conflicts of interest

There are no conflicts to declare.

Acknowledgements

Notes and references

1 L. Z. He and T. T. Dong, Progress in Controlling the Synthesis of Atomically Precise Silver Nanoclusters, *CrystEngComm*, 2021, **23**, 7369–7379.

2 R. C. Jin, C. J. Zeng, M. Zhou and Y. X. Chen, Atomically Precise Colloidal Metal Nanoclusters and Nanoparticles: Fundamentals and Opportunities, *Chem. Rev.*, 2016, **116**, 10346–10413.

3 I. Chakraborty and T. Pradeep, Atomically Precise Clusters of Noble Metals: Emerging Link between Atoms and Nanoparticles, *Chem. Rev.*, 2017, **117**, 8208–8271.

4 T. Kawawaki, Y. Negishi and H. Kawasaki, Photo/Electrocatalysis and Photosensitization Using Metal Nanoclusters for Green Energy and Medical Applications, *Nanoscale Adv.*, 2020, **2**, 17–36.

5 K. Kwak and D. Lee, Electrochemistry of Atomically Precise Metal Nanoclusters, *Acc. Chem. Res.*, 2019, **52**, 12–22.

6 Y. M. Wang, J. Cai, Q. Y. Wang, Y. Li, Z. Han, S. Li, C. H. Gong, S. Wang, S. Q. Zang and T. C. W. Mak, Electropolymerization of Metal Clusters Establishing a Versatile Platform for Enhanced Catalysis Performance, *Angew. Chem., Int. Ed.*, 2022, **61**, e202114538.

7 A. K. Deb, B. Biswas, R. Naidu and M. M. Rahman, Mechanistic Insights of Hexavalent Chromium Remediation by Halloysite-Supported Copper Nanoclusters, *J. Hazard. Mater.*, 2022, **421**, 126812.

8 V. Subramanian, S. Jena, D. Ghosh, M. Jash, A. Baksi, D. Ray and T. Pradeep, Dual Probe Sensors Using Atomically Precise Noble Metal Clusters, *ACS Omega*, 2017, **2**, 7576–7583.

9 B. J. Shi, L. Shang, W. Zhang, L. P. Jia, R. N. Ma, Q. W. Xue and H. S. Wang, Electrochemical Stripping Chemiluminescent Sensor Based on Copper Nanoclusters for Detection of Carcinoembryonic Antigen, *Sens. Actuators, B*, 2021, **344**, 130291.

10 C. Zhang, X. B. Gao, W. R. Chen, M. He, Y. Yu, G. B. Gao and T. L. Sun, Advances of Gold Nanoclusters for Bioimaging, *iScience*, 2022, **25**, 105022.

11 T. T. Jia, G. Yang, S. J. Mo, Z. Y. Wang, B. J. Li, W. Ma, Y. X. Guo, X. Chen, X. Zhao, J. Q. Liu and S. Q. Zang, Atomically Precise Gold-Levonorgestrel Nanocluster as a Radiosensitizer for Enhanced Cancer Therapy, *ACS Nano*, 2019, **13**, 8320–8328.

12 H. G. Zhu, N. W. Liu, Z. P. Wang, Q. Xue, Q. Wang, X. M. Wang, Y. Liu, Z. M. Yin and X. Yuan, Marrying Luminescent Au Nanoclusters to TiO$_2$ for Visible-Light-Driven Antibacterial Application, *Nanoscale*, 2021, **13**, 18996–19003.

13 N. W. Liu, Y. C. Wang, Z. P. Wang, Q. X. He, Y. Liu, X. Y. Dou, Z. M. Yin, Y. Li, H. G. Zhu and X. Yuan, Conjugating AIE-Featured AuAg Nanoclusters with Highly Luminescent Carbon Dots for Improved Visible-Light-Driven Antibacterial Activity, *Nanoscale*, 2022, **14**, 8183–8191.

14 W. J. Du, S. Jin, L. Xiong, M. Chen, J. Zhang, X. J. Zou, Y. Pei, S. X. Wang and M. Z. Zhu, Ag$_{50}$(Dppm)$_6$(SR)$_{30}$ and Its Homologue Au$_x$Ag$_{50-x}$(Dppm)$_6$(SR)$_{30}$ Alloy Nanocluster: Seeded Growth, Structure Determination, and Differences in Properties, *J. Am. Chem. Soc.*, 2017, **139**, 1618–1624.

15 M. S. Bootharaju, H. Chang, G. C. Deng, S. Malola, W. Baek, H. Hakkinen, N. F. Zheng and T. Hyeon, Cd$_{12}$Ag$_{32}$(SePh)$_{36}$: Non-Noble Metal Doped Silver Nanoclusters, *J. Am. Chem. Soc.*, 2019, **141**, 8422–8425.

16 H. Hirai, S. Takano, T. Nakamura and T. Tsukuda, Understanding Doping Effects on Electronic Structures of Gold Superatoms: A Case Study of Diphosphine-Protected M@Au$_{12}$ (M = Au, Pt, Ir), *Inorg. Chem.*, 2020, **59**, 17889–17895.

17 S. Takano, H. Hirai, S. Muramatsu and T. Tsukuda, Hydride-Doped Gold Superatom (Au$_9$H)$^{2+}$: Synthesis, Structure, and Transformation, *J. Am. Chem. Soc.*, 2018, **140**, 8380–8383.

18 S. L. Zhuang, L. W. Liao, M. B. Li, C. H. Yao, Y. Zhao, H. W. Dong, J. Li, H. T. Deng, L. L. Li and Z. K. Wu, The fcc Structure Isomerization in Gold Nanoclusters, *Nanoscale*, 2017, **9**, 14809–14813.

19 Q. Zhou, S. Kaappa, S. Malola, H. Lu, D. Guan, Y. J. Li, H. C. Wang, Z. X. Xie, Z. B. Ma, H. Häkkinen, N. F. Zheng, X. M. Yang and L. S. Zheng, Real-Space Imaging with Pattern Recognition of a Ligand-Protected Ag$_{374}$ Nanocluster at Sub-Molecular Resolution, *Nat. Commun.*, 2018, **9**, 2948.

20 Y. X. Du, H. T. Sheng, D. Astruc and M. Z. Zhu, Atomically Precise Noble Metal Nanoclusters as Efficient Catalysts: A Bridge between Structure and Properties, *Chem. Rev.*, 2020, **120**, 526–622.

21 Y. T. Cao, T. K. Chen, Q. F. Yao and J. P. Xie, Diversification of Metallic Molecules through Derivatization Chemistry of Au$_{25}$ Nanoclusters, *Acc. Chem. Res.*, 2021, **54**, 4142–4153.

22 L. S. Luo, Z. Y. Liu, X. S. Du and R. C. Jin, Near-Infrared Dual Emission from the Au$_{42}$(SR)$_{32}$ Nanocluster and Tailoring of Intersystem Crossing, *J. Am. Chem. Soc.*, 2022, **144**, 19243–19247.

23 M. S. Bootharaju, S. Lee, G. Deng, S. Malola, W. Baek, H. Hakkinen, N. Zheng and T. Hyeon, Ag$_{44}$(EBT)$_{26}$(TPP)$_4$ Nanoclusters with Tailored Molecular and Electronic Structure, *Angew. Chem., Int. Ed.*, 2021, **60**, 9038–9044.

24 X. Q. Liang, Y. Z. Li, Z. Wang, S. S. Zhang, Y. C. Liu, Z. Z. Cao, L. Feng, Z. Y. Gao, Q. W. Xue, C. H. Tung and D. Sun, Revealing the Chirality Origin and Homochirality Crystallization of Ag$_{14}$ Nanocluster at the Molecular Level, *Nat. Commun.*, 2021, **12**, 4966.

25 A. K. Das, S. Mukherjee, A. S. Nair, S. Bhandary, D. Chopra, D. Sanyal, B. Pathak and S. Mandal, Defects Engineering on Ceria and C–C Coupling Reactions Using [Au$_{11}$(P-Ph$_3$)$_7$I$_3$] Nanocluster: A Combined Experimental and Theoretical Study, *ACS Nano*, 2020, **14**, 16681–16688.

26 H. Shen, S. J. Xiang, Z. Xu, C. Liu, X. H. Li, C. F. Sun, S. C. Lin, B. K. Teo and N. F. Zheng, Superatomic Au$_{13}$ Clusters Ligated by Different N-Heterocyclic Carbenes and Their Ligand-Dependent Catalysis, Photoluminescence, and Proton Sensitivity, *Nano Res.*, 2020, **13**, 1908–1911.

27 M. R. Narouz, K. M. Osten, P. J. Unsworth, R. W. Y. Man, K. Salorinne, S. Takano, R. Tomihara, S. Kaappa, S. Malola, C. T. Dinh, J. D. Padmos, K. Ayoo, P. J. Garrett, M. Nambo, J. H. Horton, E. H. Sargent, H. Hakkinen, T. Tsukuda and C. M. Crudden, N-Heterocyclic Carbene-Functionalized Magic-Number Gold Nanoclusters, *Nat. Chem.*, 2019, **11**, 419–425.

28 S. F. Yuan, C. Q. Xu, W. D. Liu, J. X. Zhang, J. Li and Q. M. Wang, Rod-Shaped Silver Supercluster Unveiling Strong Electron Coupling between Substituent Icosahedral Units, *J. Am. Chem. Soc.*, 2021, **143**, 12261–12267.

29 S. F. Yuan, W. D. Liu, C. Y. Liu, Z. J. Guan and Q. M. Wang, Nitrogen Donor Protection for Atomically Precise Metal Nanoclusters, *Chem. – Eur. J.*, 2022, **28**, e202104445.

30 Z. J. Guan, F. Hu, J. J. Li, Z. R. Liu and Q. M. Wang, Homoleptic Alkynyl-Protected Gold Nanoclusters with Unusual Compositions and Structures, *Nanoscale*, 2020, **12**, 13346–13350.

31 W. D. Liu, J. Q. Wang, S. F. Yuan, X. Chen and Q. M. Wang, Chiral Superatomic Nanoclusters Ag$_{47}$ Induced by the Ligation of Amino Acids, *Angew. Chem., Int. Ed.*, 2021, **60**, 11430–11435.

32 F. Hu, J. J. Li, Z. J. Guan, S. F. Yuan and Q. M. Wang, Formation of an Alkynyl-Protected Ag112 Silver Nanocluster as Promoted by Chloride Released In Situ from CH$_2$Cl$_2$, *Angew. Chem., Int. Ed.*, 2020, **59**, 5312–5315.

33 X. S. Ma, Y. Tang, G. Y. Ma, L. B. Qin and Z. H. Tang, Controllable Synthesis and Formation Mechanism Study of Homoleptic Alkynyl-Protected Au Nanoclusters: Recent Advances, Grand Challenges, and Great Opportunities, *Nanoscale*, 2021, **13**, 602–614.

34 Z. Lei, X. K. Wan, S. F. Yuan, Z. J. Guan and Q. M. Wang, Alkynyl Approach toward the Protection of Metal Nanoclusters, *Acc. Chem. Res.*, 2018, **51**, 2465–2474.

35 Z. Lei, X. K. Wan, S. F. Yuan, J. Q. Wang and Q. M. Wang, Alkynyl-Protected Gold and Gold-Silver Nanoclusters, *Dalton Trans.*, 2017, **46**, 3427–3434.

36 E. Wang, W. W. Xu, B. Zhu and Y. Gao, Understanding the Chemical Insights of Staple Motifs of Thiolate-Protected Gold Nanoclusters, *Small*, 2021, **17**, e2001836.

37 L. Y. Chen, F. Sun, Q. L. Shen, L. B. Qin, Y. G. Liu, L. Qiao, Q. Tang, L. K. Wang and Z. H. Tang, Homoleptic Alkynyl-Protected Ag$_{32}$ Nanocluster with Atomic Precision: Probing the Ligand effect toward CO$_2$ Electroreduction and 4-Nitrophenol Reduction, *Nano Res.*, 2022, **15**, 8908–8913.

38 J. J. Li, Z. J. Guan, Z. Lei, F. Hu and Q. M. Wang, Same Magic Number but Different Arrangement: Alkynyl-Protected Au$_{25}$ with D_3 symmetry, *Angew. Chem., Int. Ed.*, 2019, **58**, 1083–1087.

39 X. K. Wan, Z. J. Guan and Q. M. Wang, Homoleptic Alkynyl-Protected Gold Nanoclusters: Au$_{44}$(PhC≡C)$_{28}$ and Au$_{36}$-(PhC≡C)$_{24}$, *Angew. Chem., Int. Ed.*, 2017, **56**, 11494–11497.

40 M. Sugiuchi, Y. Shichibu, T. Nakanishi, Y. Hasegawa and K. Konishi, Cluster-π Electronic Interaction in a Superatomic Au$_{13}$ Cluster Bearing σ-Bonded Acetylide Ligands, *Chem. Commun.*, 2015, **51**, 13519–13522.

41 X. S. Han, X. Luan, H. F. Su, J. J. Li, S. F. Yuan, Z. Lei, Y. Pei and Q. M. Wang, Structure Determination of Alkynyl-Protected Gold Nanocluster Au$_{22}$(^{t}BuC≡C)$_{18}$ and Its Thermochromic Luminescence, *Angew. Chem., Int. Ed.*, 2020, **59**, 2309–2312.

42 M. M. Zhang, X. Y. Dong, Z. Y. Wang, X. M. Luo, J. H. Huang, S. Q. Zang and T. C. Mak, Alkynyl-Stabilized Superatomic Silver Clusters Showing Circularly Polarized Luminescence, *J. Am. Chem. Soc.*, 2021, **143**, 6048–6053.

43 G. X. Duan, L. Tian, J. B. Wen, L. Y. Li, Y. P. Xie and X. Lu, An Atomically Precise All-Tert-Butylethynide-Protected Ag$_{51}$ Superatom Nanocluster with Color Tunability, *Nanoscale*, 2018, **10**, 18915–18919.

44 X. K. Wan, J. Q. Wang, Z. A. Nan and Q. M. Wang, Ligand Effects in Catalysis by Atomically Precise Gold Nanoclusters, *Sci. Adv.*, 2017, **3**, e1701823.

45 X. Li, S. Takano and T. Tsukuda, Ligand Effects on the Hydrogen Evolution Reaction Catalyzed by Au$_{13}$ and Pt@Au$_{12}$: Alkynyl vs Thiolate, *J. Phys. Chem. C*, 2021, **125**, 23226–23230.

46 Z. Lei, J. J. Li, X. K. Wan, W. H. Zhang and Q. M. Wang, Isolation and Total Structure Determination of an All-Alkynyl-Protected Gold Nanocluster Au$_{144}$, *Angew. Chem., Int. Ed.*, 2018, **57**, 8639–8643.

47 X. S. Ma, G. Y. Ma, L. B. Qin, G. X. Chen, S. W. Chen and Z. H. Tang, A Synchronous Nucleation and Passivation Strategy for Controllable Synthesis of Au$_{36}$(PA)$_{24}$: Unveiling the Formation Process and the Role of Au$_{22}$(PA)$_{18}$ Intermediate, *Sci. China: Chem.*, 2020, **63**, 1777–1784.

48 G. Y. Ma, Y. Tang, L. Y. Chen, L. B. Qin, Q. L. Shen, L. K. Wang and Z. H. Tang, A Homoleptic Alkynyl-Protected Au(I)$_9$–Ag(I)$_9$ Cluster: Structure Analysis, Optical Properties, and Catalytic Implications, *Eur. J. Inorg. Chem.*, 2022, e202200176.

49 K. Konishi, M. Iwasaki, M. Sugiuchi and Y. Shichibu, Ligand-Based Toolboxes for Tuning of the Optical Properties of Subnanometer Gold Clusters, *J. Phys. Chem. Lett.*, 2016, **7**, 4267–4274.

50 N. Kobayashi, Y. Kamei, Y. Shichibu and K. Konishi, Protonation-Induced Chromism of Pyridylethynyl-Appended [core + exo]-Type Au$_8$ Clusters. Resonance-Coupled Electronic Perturbation through π-Conjugated Group, *J. Am. Chem. Soc.*, 2013, **135**, 16078–16081.

51 S. Ito, S. Takano and T. Tsukuda, Alkynyl-Protected Au$_{22}$(C≡CR)$_{18}$ Clusters Featuring New Interfacial Motifs and R-Dependent Photoluminescence, *J. Phys. Chem. Lett.*, 2019, **10**, 6892–6896.

52 Z. J. Guan, F. Hu, J. J. Li, Z. R. Wen, Y. M. Lin and Q. M. Wang, Isomerization in Alkynyl-Protected Gold Nanoclusters, *J. Am. Chem. Soc.*, 2020, **142**, 2995–3001.

53 J. J. Li, Z. K. Liu, Z. J. Guan, X. S. Han, W. Q. Shi and Q. M. Wang, A 59-Electron Non-Magic-Number Gold Nanocluster Au$_{99}$(C≡CR)$_{40}$ Showing Unexpectedly High Stability, *J. Am. Chem. Soc.*, 2022, **144**, 690–694.

54 X. S. Ma, Z. H. Tang, L. B. Qin, J. Peng, L. G. Li and S. W. Chen, Unravelling the Formation Mechanism of Alkynyl Protected Gold Clusters: A Case Study of Phenylacetylene Stabilized Au$_{144}$ Molecules, *Nanoscale*, 2020, **12**, 2980–2986.

55 S. F. Yuan, P. Li, Q. Tang, X. K. Wan, Z. A. Nan, D. E. Jiang and Q. M. Wang, Alkynyl-Protected Silver Nanoclusters Featuring an Anticuboctahedral Kernel, *Nanoscale*, 2017, **9**, 11405–11409.

56 J. Q. Wang, S. Shi, R. L. He, S. F. Yuan, G. Y. Yang, G. J. Liang and Q. M. Wang, Total Structure Determination of the Largest Alkynyl-Protected fcc Gold Nanocluster Au$_{110}$ and the Study on Its Ultrafast Excited-State Dynamics, *J. Am. Chem. Soc.*, 2020, **142**, 18086–18092.

57 Y. Wang, X. K. Wan, L. T. Ren, H. F. Su, G. Li, S. Malola, S. C. Lin, Z. C. Tang, H. Häkkinen, B. K. Teo, Q. M. Wang and N. F. Zheng, Atomically Precise Alkynyl-Protected Metal Nanoclusters as a Model Catalyst: Observation of Promoting Effect of Surface Ligands on Catalysis by Metal Nanoparticles, *J. Am. Chem. Soc.*, 2016, **138**, 3278–3281.

58 M. Z. Zhu, E. Lanni, N. Garg, M. K. Bier and R. C. Jin, Kinetically Controlled, High-Yield Synthesis of Au_{25} Clusters, *J. Am. Chem. Soc.*, 2008, **130**, 1138–1139.

59 X. Kang and M. Z. Zhu, Transformation of Atomically Precise Nanoclusters by Ligand-Exchange, *Chem. Mater.*, 2019, **31**, 9939–9969.

60 W. Suzuki, R. Takahata, Y. Chiga, S. Kikkawa, S. Yamazoe, Y. Mizuhata, N. Tokitoh and T. Teranishi, Control over Ligand-Exchange Positions of Thiolate-Protected Gold Nanoclusters Using Steric Repulsion of Protecting Ligands, *J. Am. Chem. Soc.*, 2022, **144**, 12310–12320.

61 Y. Zeng, S. Havenridge, M. Gharib, A. Baksi, K. L. D. M. Weerawardene, A. R. Ziefuss, C. Strelow, C. Rehbock, A. Mews, S. Barcikowski, M. M. Kappes, W. J. Parak, C. M. Aikens and I. Chakraborty, Impact of Ligands on Structural and Optical Properties of Ag_{29} Nanoclusters, *J. Am. Chem. Soc.*, 2021, **143**, 9405–9414.

62 P. Maity, H. Tsunoyama, M. Yamauchi, S. Xie and T. Tsukuda, Organogold Clusters Protected by Phenylace-tylene, *J. Am. Chem. Soc.*, 2011, **133**, 20123–20125.

63 S. Takano, S. Ito and T. Tsukuda, Efficient and Selective Conversion of Phosphine-Protected $(MAu_8)^{2+}$ (M = Pd, Pt) Superatoms to Thiolate-Protected $(MAu_{12})^{6+}$ or Alkynyl-Protected $(MAu_{12})^{4+}$ Superatoms via Hydride Doping, *J. Am. Chem. Soc.*, 2019, **141**, 15994–16002.

64 C. A. Hosier, I. D. Anderson and C. J. Ackerson, Acetylide-for-Thiolate and Thiolate-for-Acetylide Exchange on Gold Nanoclusters, *Nanoscale*, 2020, **12**, 6239–6242.

65 Y. B. Ma, J. Wang, J. L. Yu, J. W. Zhou, X. C. Zhou, H. X. Li, Z. He, H. W. Long, Y. H. Wang, P. Y. Lu, J. W. Yin, H. Y. Sun, Z. C. Zhang and Z. X. Fan, Surface Modification of Metal Materials for High-Performance Electrocatalytic Carbon Dioxide Reduction, *Matter*, 2021, **4**, 888–926.

66 Z. Xin, J. Liu, X. Wang, K. Shen, Z. Yuan, Y. Chen and Y. Q. Lan, Implanting Polypyrrole in Metal-Porphyrin MOFs: Enhanced Electrocatalytic Performance for CO_2RR, *ACS Appl. Mater. Interfaces*, 2021, **13**, 54959–54966.

67 L. B. Qin, G. Y. Ma, L. K. Wang and Z. H. Tang, Atomically Precise Metal Nanoclusters for (Photo)Electroreduction of CO_2: Recent Advances, Challenges and Opportunities, *J. Energy Chem.*, 2021, **57**, 359–370.

68 Y. B. Ma, J. L. Yu, M. Z. Sun, B. Chen, X. C. Zhou, C. L. Ye, Z. Q. Guan, W. H. Guo, G. Wang, S. Y. Lu, D. S. Xia, Y. H. Wang, Z. He, L. Zheng, Q. B. Yun, L. Q. Wang, J. W. Zhou, P. Y. Lu, J. W. Yin, Y. F. Zhao, Z. B. Luo, L. Zhai, L. W. Liao, Z. L. Zhu, R. Q. Ye, Y. Chen, Y. Lu, S. B. Xi, B. L. Huang, C. S. Lee and Z. X. Fan, Confined Growth of Silver-Copper Janus Nanostructures with {100} Facets for Highly Selective Tandem Electrocatalytic Carbon Dioxide Reduction, *Adv. Mater.*, 2022, **34**, e2110607.

69 B. Xiong, J. Liu, Y. J. Yang, Y. C. Yang and Z. X. Hua, Effect Mechanism of NO on Electrocatalytic Reduction of CO_2 to CO over Pd@Cu Bimetal Catalysts, *Fuel*, 2022, **323**, 124339.

70 M. M. Ayyub and C. N. R. Rao, Designing Electrode Materials for the Electrochemical Reduction of Carbon Dioxide, *Mater. Horiz.*, 2021, **8**, 2420–2443.

71 X. Z. Lin, W. G. Ma, K. J. Sun, B. Sun, X. M. Fu, X. Q. Ren, C. Liu and J. H. Huang, $[AuAg_{26}(SR)_{18}S]^-$ Nanocluster: Open Shell Structure and High faradaic Efficiency in Electrochemical Reduction of CO_2 to CO, *J. Phys. Chem. Lett.*, 2021, **12**, 552–557.

72 W. Choi, H. Seong, V. Efremov, Y. Lee, S. Im, D. H. Lim, J. S. Yoo and D. Lee, Controlled Syngas Production by Electrocatalytic CO_2 Reduction on Formulated $Au_{25}(SR)_{18}$ and $PtAu_{24}(SR)_{18}$ Nanoclusters, *J. Chem. Phys.*, 2021, **155**, 014305.

73 Z. H. Gao, K. Wei, T. Wu, J. Dong, D. E. Jiang, S. Sun and L. S. Wang, A Heteroleptic Gold Hydride Nanocluster for Efficient and Selective Electrocatalytic Reduction of CO_2 to CO, *J. Am. Chem. Soc.*, 2022, **144**, 5258–5262.

74 V. K. Kulkarni, B. N. Khiarak, S. Takano, S. Malola, E. L. Albright, T. I. Levchenko, M. D. Aloisio, C. T. Dinh, T. Tsukuda, H. Hakkinen and C. M. Crudden, N-Heterocyclic Carbene-Stabilized Hydrido Au_{24} Nanoclusters: Synthesis, Structure, and Electrocatalytic Reduction of CO_2, *J. Am. Chem. Soc.*, 2022, **144**, 9000–9006.

75 J. Y. Xu, L. Xiong, X. Cai, S. S. Tang, A. C. Tang, X. Liu, Y. Pei and Y. Zhu, Evolution from Superatomic $Au_{24}Ag_{20}$ Monomers into Molecular-Like $Au_{43}Ag_{38}$ Dimeric Nanoclusters, *Chem. Sci.*, 2022, **13**, 2778–2782.

76 S. S. Tang, J. Y. Xu, X. Liu and Y. Zhu, Ag Doped Au_{44} Nanoclusters for Electrocatalytic Conversion of CO_2 to CO, *Chem. – Eur. J.*, 2022, **28**, e202201262.

77 D. R. Kauffman, D. Alfonso, C. Matranga, H. F. Qian and R. C. Jin, Experimental and Computational Investigation of Au_{25} Clusters and CO_2: A Unique Interaction and Enhanced Electrocatalytic Activity, *J. Am. Chem. Soc.*, 2012, **134**, 10237–10243.

78 S. Li, D. Alfonso, A. V. Nagarajan, S. D. House, J. C. Yang, D. R. Kauffman, G. Mpourmpakis and R. C. Jin, Mono-palladium Substitution in Gold Nanoclusters Enhances CO_2 Electroreduction Activity and Selectivity, *ACS Catal.*, 2020, **10**, 12011–12016.

79 S. Zhao, N. Austin, M. Li, Y. B. Song, S. D. House, S. Bernhard, J. C. Yang, G. Mpourmpakis and R. C. Jin, Influence of Atomic-Level Morphology on Catalysis: The Case of Sphere and Rod-Like Gold Nanoclusters for CO_2 Electroreduction, *ACS Catal.*, 2018, **8**, 4996–5001.

80 D. R. Kauffman, D. Alfonso, C. Matranga, P. Ohodnicki, X. Y. Deng, R. C. Siva, C. J. Zeng and R. C. Jin, Probing Active Site Chemistry with Differently Charged Au_{25}^q Nanoclusters (q = −1, 0, +1), *Chem. Sci.*, 2014, **5**, 3151–3157.

81 H. Seong, V. Efremov, G. Park, H. Kim, J. S. Yoo and D. Lee, Atomically Precise Gold Nanoclusters as Model Catalysts for Identifying Active Sites for Electroreduction of CO_2, *Angew. Chem., Int. Ed.*, 2021, **60**, 14563–14570.

82 S. L. Zhuang, D. Chen, L. W. Liao, Y. Zhao, N. Xia, W. H. Zhang, C. M. Wang, J. Yang and Z. K. Wu, Hard-Sphere Random Close-Packed Au47Cd2(TBBT)31 Nanoclusters with a faradaic Efficiency of Up to 96% for Electrocatalytic CO2 Reduction to CO, *Angew. Chem., Int. Ed.*, 2020, **59**, 3073–3077.

83 Y. N. Sun, X. Liu, K. Xiao, Y. Zhu and M. Y. Chen, Active-Site Tailoring of Gold Cluster Catalysts for Electrochemical CO_2 Reduction, *ACS Catal.*, 2021, **11**, 11551–11560.

84 N. Austin, S. Zhao, J. R. McKone, R. C. Jin and G. Mpourmpakis, Elucidating the Active Sites for CO_2 Electroreduction on Ligand-Protected Au_{25} Nanoclusters, *Catal. Sci. Technol.*, 2018, **8**, 3795–3805.

85 X. K. Wan, J. Q. Wang and Q. M. Wang, Ligand-Protected Au_{55} with a Novel Structure and Remarkable CO_2 Electroreduction Performance, *Angew. Chem., Int. Ed.*, 2021, **60**, 20748–20753.

86 S. F. Yuan, R. L. He, X. S. Han, J. Q. Wang, Z. J. Guan and Q. M. Wang, Robust Gold Nanocluster Protected with Amidinates for Electrocatalytic CO_2 Reduction, *Angew. Chem., Int. Ed.*, 2021, **60**, 14345–14349.

87 D. Yang, J. W. Wang, Q. J. Wang, Z. T. Yuan, Y. H. Dai, C. M. Zhou, X. Y. Wan, Q. C. Zhang and Y. H. Yang, Electrocatalytic CO_2 Reduction over Atomically Precise Metal Nanoclusters Protected by Organic Ligands, *ACS Nano*, 2022, **16**, 15681–15704.

88 S. Zhao, R. X. Jin and R. C. Jin, Opportunities and Challenges in CO_2 Reduction by Gold- and Silver-Based Electrocatalysts: From Bulk Metals to Nanoparticles and Atomically Precise Nanoclusters, *ACS Energy Lett.*, 2018, **3**, 452–462.

89 L. B. Qin, F. Sun, X. S. Ma, G. Y. Ma, Y. Tang, L. K. Wang, Q. Tang, R. C. Jin and Z. H. Tang, Homoleptic Alkynyl-Protected Ag_{15} Nanocluster with Atomic Precision: Structural Analysis and Electrocatalytic Performance toward CO_2 Reduction, *Angew. Chem., Int. Ed.*, 2021, **60**, 26136–26141.

90 A. Ghosh, O. F. Mohammed and O. M. Bakr, Atomic-Level Doping of Metal Clusters, *Acc. Chem. Res.*, 2018, **51**, 3094–3103.

91 S. X. Wang, Q. Li, X. Kang and M. Z. Zhu, Customizing the Structure, Composition, and Properties of Alloy Nanoclusters by Metal Exchange, *Acc. Chem. Res.*, 2018, **51**, 2784–2792.

92 Z. B. Gan, N. Xia and Z. K. Wu, Discovery, Mechanism, and Application of Antigalvanic Reaction, *Acc. Chem. Res.*, 2018, **51**, 2774–2783.

93 Y. Wang, H. F. Su, L. T. Ren, S. Malola, S. C. Lin, B. K. Teo, H. Hakkinen and N. F. Zheng, Site Preference in Multimetallic Nanoclusters:Incorporation of Alkali Metal Ions or Copper Atoms into the Alkynyl-Protected BodyCentered Cubic Cluster $[Au_7Ag_8(C≡C^tBu)_{12}]$, *Angew. Chem., Int. Ed.*, 2016, **55**, 15152–15156.

94 X. S. Ma, L. Xiong, L. B. Qin, Y. Tang, G. Y. Ma, Y. Pei and Z. H. Tang, A Homoleptic Alkynyl-Protected $[Ag_9Cu_6(t-BuC≡C)_{12}]^+$ Superatom with Free Electrons: Synthesis, Structure Analysis, and Different Properties Compared with the Au7Ag8 Cluster in the $M_{15}{}^+$ Series, *Chem. Sci.*, 2021, **12**, 12819–12826.

95 X. S. Ma, F. Sun, L. B. Qin, Y. G. Liu, X. W. Kang, L. K. Wang, D. E. Jiang, Q. Tang and Z. H. Tang, Electrochemical CO_2 Reduction Catalyzed by Atomically Precise Alkynyl-Protected Au_7Ag_8, Ag_9Cu_6, and $Au_2Ag_8Cu_5$ Nanoclusters: Probing the Effect of Multi-Metal Core on Selectivity, *Chem. Sci.*, 2022, **13**, 10149–10158.

96 S. Li, A. V. Nagarajan, Y. Li, D. R. Kauffman, G. Mpourmpakis and R. C. Jin, The Role of Ligands in Atomically Precise Nanocluster-Catalyzed CO_2 Electrochemical Reduction, *Nanoscale*, 2021, **13**, 2333–2337.

97 J. Wang, F. Xu, Z. Y. Wang, S. Q. Zang and T. C. W. Mak, Ligand-Shell Engineering of a Au_{28} Nanocluster Boosts Electrocatalytic CO_2 Reduction, *Angew. Chem., Int. Ed.*, 2022, **61**, e202207492.

98 J. J. Li, Z. J. Guan, S. F. Yuan, F. Hu and Q. M. Wang, Enriching Structural Diversity of Alkynyl-Protected Gold Nanoclusters with Chlorides, *Angew. Chem., Int. Ed.*, 2021, **60**, 6699–6703.

99 M. Qu, H. Li, L. H. Xie, S. T. Yan, J. R. Li, J. H. Wang, C. Y. Wei, Y. W. Wu and X. M. Zhang, Bidentate Phosphine-Assisted Synthesis of an All-Alkynyl-Protected Ag_{74} Nanocluster, *J. Am. Chem. Soc.*, 2017, **139**, 12346–12349.

100 B. L. Han, Z. Liu, L. Feng, Z. Wang, R. K. Gupta, C. M. Aikens, C. H. Tung and D. Sun, Polymorphism in Atomically Precise Cu_{23} Nanocluster Incorporating Tetrahedral $[Cu_4]^0$ Kernel, *J. Am. Chem. Soc.*, 2020, **142**, 5834–5841.

101 X. K. Wan, X. L. Cheng, Q. Tang, Y. Z. Han, G. Hu, D. E. Jiang and Q. M. Wang, Atomically Precise Bimetallic $Au_{19}Cu_{30}$ Nanocluster with an Icosidodecahedral Cu_{30} Shell and an Alkynyl-Cu Interface, *J. Am. Chem. Soc.*, 2017, **139**, 9451–9454.

102 H. Shen and T. Mizuta, An Alkynyl-Stabilized Pt_5Ag_{22} Cluster Featuring a Two-Dimensional Alkynyl-Platinum "Crucifix Motif", *Chem. – Eur. J.*, 2017, **23**, 17885–17888.

103 Q. Tang, Y. J. Lee, D. Y. Li, W. J. Choi, C. W. Liu, D. Lee and D. E. Jiang, Lattice-Hydride Mechanism in Electrocatalytic CO_2 Reduction by Structurally Precise Copper-Hydride Nanoclusters, *J. Am. Chem. Soc.*, 2017, **139**, 9728–9736.

104 D. M. Chevrier, L. Raich, C. Rovira, A. Das, Z. T. Luo, Q. F. Yao, A. Chatt, J. P. Xie, R. C. Jin, J. Akola and P. Zhang, Molecular-Scale Ligand Effects in Small Gold-Thiolate Nanoclusters, *J. Am. Chem. Soc.*, 2018, **140**, 15430–15436.

105 X. D. Liu, H. Y. Yang, Y. X. Chen, Y. Yang, L. Porcar, A. Radulescu, S. Guldin, R. C. Jin, F. Stellacci and Z. Luo, Quantifying the Solution Structure of Metal Nanoclusters Using Small-Angle Neutron Scattering, *Angew. Chem., Int. Ed.*, 2022, **61**, e202209751.